Dynamic Detection Method of Medium-Low Speed Maglev F-Track seams Based on Machine Vision

Dongkai Zhang, Shibin Gao, Long Yu, Dong Zhan

Abstract— **This paper presents a dynamic detection method of medium and low speed maglev F-track seam based on machine vision detection technology. A Kalman filter light bar center extraction algorithm based on ridge line prediction is proposed for the bar image of F-track seam detection. And a threshold segmentation feature point extraction method is proposed for the center of the light bar. The static and dynamic precision of detection system are verified by the stability test, static and dynamic precision test. The static detection accuracy of end of F-track seam is less than 0.5mm and dynamic detection accuracy is less than 0.8mm. Then the static precision is less than 0.2mm the dynamic accuracy is less than 0.5mm about the horizontal F-track seam. And the static precision is less than 0.2mm, and the dynamic accuracy is less than 0.5mm about the vertical F-track seam. The detection accuracy of the system meets the requirements of F-track seam precision.**

Index Terms—**F-Track, feature points, kalmam, light bar center, seam.**

I. INTRODUCTION

In China the medium-low speed maglev railway system mainly adopts electromagnetic attraction levitation mode. And ideally, the levitation gap of the maglev train is kept within the design range. However, the irregular track will reduce the magnetic levitation system stability of maglev train, such as increased fluctuation of the levitation gap [1]. In the many factors that cause track irregularity, the unevenness of the magnetic F-track seam has a great influence on the magnetic levitation system stability of maglev train. Therefore, it is very important for the line maintenance and the stable operation of maglev train to study the method of F-track seam detection.

In the [2], a kind of hand-push medium-low speed maglev F-track static geometric detector is proposed, which can realize the detection of geometric parameters such as mileage, gauge, longitudinal level, alignment F-track seam etc. And the function of hand-push detection equipment is relatively comprehensive but the detection efficiency of the equipment is low. In addition it is dangerous to push the equipment in the medium-low speed magnetic overhead lines. In [3-4], a method for detecting long-wave irregularity of maglev tracks based on inertial method is proposed. In [5], a geometric parameter detection system FMS01 is proposed. The system is mounted on a maglev train bogie and detects geometrical parameters such as gauge, longitudinal level cross level and alignment geometric parameters based on inertial principle. However, the dynamic detection method proposed in [3-4] and [5] is mainly used to detect the longitudinal and cross level of F-track, and can not detect the F-track seam defects. Therefore, this paper presents a method of F-track seam measurement based on machine vision, which is of great significance to the scientific maintenance of medium-low speed maglev F-track.

Machine vision measurement technology is widely used in the field of rail traffic detection. The GJ-6 type railway detection system discussed in [6] is based on the visual measurement technique and the inertial datum method to detect the geometrical irregularity of the track. And the tunnel clearance detection system, catenary geometric parameters of high-speed dynamic detection method and rail wear cross-sectional area measurement methods based on the visual measurement technology have been studied in [7-10]. The application of these detection methods achieved great results in the field of rail transportation. In the visual measurement technology, the light bar center and feature extraction is one of the key technologies. In the high-speed dynamic detection using structured light technology, the improved gray-scale gravity center method is often used to extract the light bar center [11] and combine the filtering algorithm to smooth the center. It can reduce noise interference. However, these filtering methods maybe increase the light bar center extraction error. Because it always lead to the center of the light bar to offset in the inflection point. In this paper, a Kalman filter light bar center extraction method based on ridge line prediction and a threshold segmentation feature point extraction method are proposed for F-track seam image processing.

II. THE GEOMETRICAL PARAMETERS OF MEDIUM-LOW MAGLEV TRACK

The track of medium-low speed maglev was "F" type, so it is

Dongkai Zhang received the B.S. degree in electrical engineering from Henan University of Science and Technology, LuoYang, China, in 2010, and the M.S. degree in Electrical Engineering from Southwest Jiaotong University, Chengdu, China, where he is currently working toward Ph.D. degree in Electrical Engineering. (e-mail: fengmituzi@163.com)

Shibin Gao received the B.S., M.S. and Ph.D. degrees in Electrical Engineering from Southwest Jiaotong University, Chengdu, China, in 1985, 1988 and 2004, respectively. (e-mail: gao_shi_bin@126.com)

Long Yu received the B.S., M.S. and Ph.D. degrees in Electrical Engineering from Southwest Jiaotong University, Chengdu, China, in 2003, 2006 and 2008, respectively. (e-mail: yulong.swjtu@163.com)

Dong Zhan received the B.S. degree in electrical engineering from Jiangxi University of Science and Technology, Nan Chang, China, in 2009, and the M.S. and Ph.D degrees in electrical engineering from Southwest Jiaotong University, Chengdu, China, in 2012 and 2016, respectively. (e-mail: 15198281626@163.com)

also referred to as the F-track, which consists of linear motor induction plate, suspension clearance detection surface, the internal magnetic pole surface, the external magnetic pole surface and the running surface composition, as shown in Fig.1.

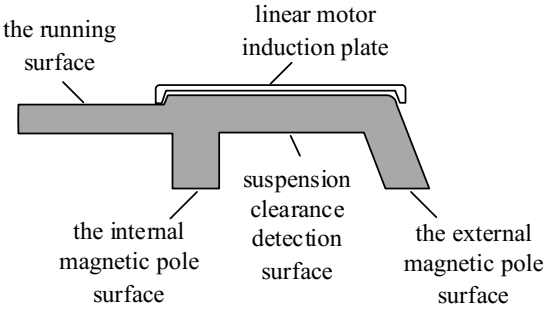

Fig. 1. Medium-low speed maglev F-track.

The static geometrical parameters of the middle-low speed maglev track include the parameters such as gauge, magnetic, longitudinal level, alignment, cross level, curvature and F-track seam etc [12]. This paper mainly study on the F-track seam detection method, so this section mainly discusses the F-track seam parameters.

The medium-low speed maglev line consists of multi-segment tracks, and there is gap between the two tracks, as shown in Fig. 2.

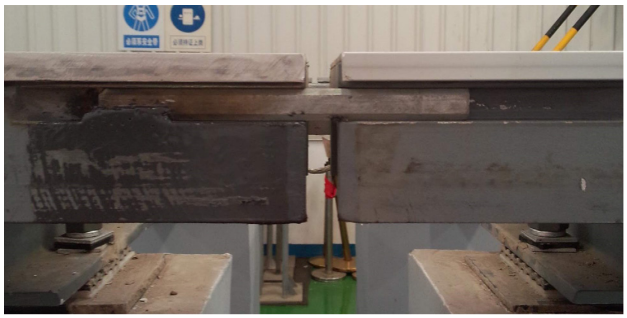

Fig. 2. Medium-low speed maglev F-track pictures.

The geometrical parameters of the seam are divided into horizontal F-track seam, vertical F-track seam and end of F-track seam according to different spatial position misalignment, as shown in Fig. 3. The horizontal F-track seam can be defined as the deviation of the two F-track seam in the horizontal direction, as $C'D'$ shown in Fig. 3. Then the vertical F-track seam can be defined as the height deviation of the two F-track seam in the vertical direction, as AB' shown in Fig. 3. And the end of F-track seam can be defined as the gap width between the two tracks in the direction of travel, as BB' shown in Fig. 3.

The geometrical parameters of the seam are very important. For example, if the deviation of the horizontal rail seam is too large, it will cause the maglev train to collide with the side of the track when passing F-track seams. Moreover if vertical deviation of the track is too large, it will cause the maglev train to shake when it passes through the F-track seam, and the train body is prone to collide with the linear motor induction plate or the internal and external magnetic pole surface. And if the end of the F-track seam is too small, the track is prone to deformation because of the thermal expansion and contraction. And it will influence the stability of the maglev train suspension control system, if the end of the F-track seam is too wide [15].

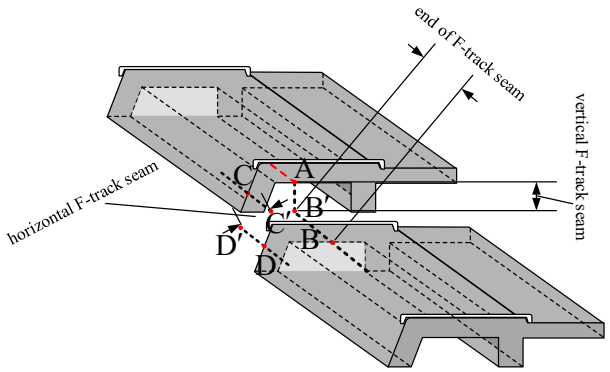

Fig. 3. Geometrical parameters of F-track seam.

III. F-TRACK SEAM DETECTION SYSTEM

A. *The structure of detection system*

The detection system mounted on the comprehensive inspection vehicles of medium-low speed maglev for dynamic detection purposes, which mainly include measuring racks, sensors and central processing system, as shown in Fig. 4.

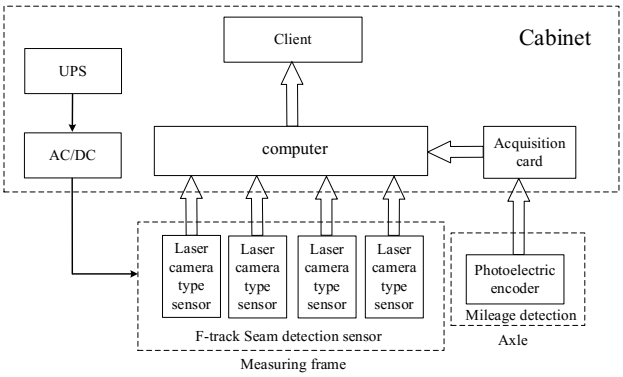

Fig. 4. Detection system block diagram.

The detection system is built on the basis of the laser camera sensor. The detection image collected by the sensor is transmitted to the computer, then the geometric parameters of the F-track seam are calculated according to the detection image, and combined the mileage information which collected by photoelectric encoder sensor to locate the seam location . The final detection information is uploaded to the client for display and report generation.

B. *Detection principle*

Medium-low speed maglev F-track seam detection is realized through four laser camera sensor. The laser camera is a sensor designed based on the machine vision detection principle. It is mainly composed of a laser and a CCD camera. The camera captures the laser image projected on the target surface and calculates the required geometric parameters by processing the image. The camera in the laser camera sensor need to be calibrated to establish the correspondence between the camera image coordinate system and the world coordinate

system. In this paper, we use the camera nonlinear model described in [13] to calibrate the dynamic detection system.

The sensor distribution is shown in Fig. 5. The horizontal track detection sensor L_1 and R_1 is located on the side of the external magnetic pole of the F-track. The laser plane horizontally illuminates the outer side of the external magnetic pole to form a laser light bar in the direction of the track, as shown in Fig. 6. The camera captures the light bar which contains information about the geometric parameters of F-track seam to detect the horizontal track seam. The vertical F-track seam and the end of the F-track seam detection sensors L_2 and R_2 located on just below suspension clearance detection surface of F-track. The laser plane illuminates the suspension clearance detection surface vertically and forms a light bar in the direction of the track. The camera takes the light bar, which is modulated by the F-track seam, to detect the vertical and the end of F-track seam, as shown in Fig. 7. The distance between the sensor and the track seam is 200mm, and the influence of the vibration of the vehicle body on the detection result is negligible. Sensor camera acquisition frequency of 200 f/s, the laser light bar effective length is 200mm and the design width of track seam is generally 20mm. therefore the detection system can adapt to the detection rate of 30km/h without missing phenomenon.

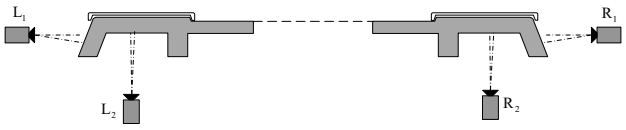

Fig. 5. Sensor distribution.

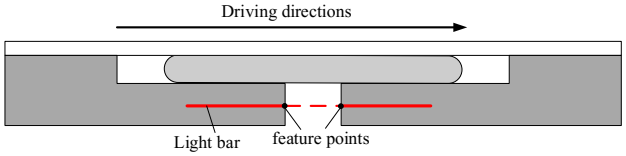

Fig. 6. Horizontal F-track seam laser distribution.

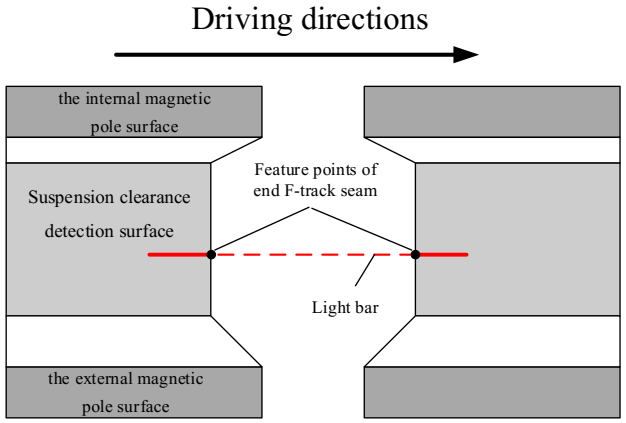

Fig. 7. Vertical and end F-track seam laser distribution.

IV. Light Bar Center Extraction Method

At present, the main light bar center extraction algorithm is the Steger method, ridge tracking method and gray center of gravity method. And Steger method and ridge tracking method is more accurate than gray center of gravity method. However, these two algorithms are computationally intensive and difficult to meet real-time requirements. If the normal grayscale method is used to deal with light bars with wide width and wide noise at the larger edges of the saturated region, the center of the light bars which is extracted will appear obvious jagged, as shown in Fig.8.

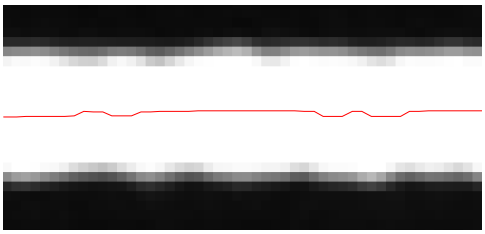

Fig. 8. Light bar center extract partial magnification.

Aiming at the above problem, this paper proposes a Kalman filter light bar center extraction method based on ridge line prediction. The main idea of the algorithm is to calculate the initial ridge direction of the light bar through the edge detection operator, and then calculate the predicted value of the center point of the light bar according to the initial ridge direction of the light bar, and then calculate the observation value of the prediction point, and then the Kalman filter is used to obtain the center of the light bar. Finally, the next step of the ridge line direction algorithm is predicted according to the extracted light bar center data, and the above process is repeated. The main steps are as follows:

Step 1: Ridge direction initialization

Select the light bar starting column gray center of gravity as the initial point S_0, the initial point edge gradient direction is calculated by the Sobel operator to obtain the initial ridge line direction θ_{l_0} as the initial ridge direction for the light bar center prediction.

Step 2: Update the prediction center

S_{k-1} point is the current point, S_{k-1} point corresponding to the ridge direction for the θ_{k-1}, from the S_{k-1} point along the ridge direction θ_{k-1} forward d pixels to reach P_k point. It is the step k prediction center point.

Step 3: Light bar center observation point extraction

According to the ridge line direction θ_k of point P_k, the normal direction $\varphi_k = \theta_k + \pi/2$ is obtained. The gray-scale curve distribution $G(i)$ $(i = 1, 2, \cdots, 2n+1)$ is obtained along the normal direction φ_k with the point P_k as the center, and the grayscale center of grayscale curve $G(i)$ is used as the center point Z_k of the updated light bar.

Step 4: Light bar center point extraction

The Kalman filter model is constructed for the extraction process of the light bar, and the state space is described as (1).

$$\begin{cases} X(k) = AX(k-1) + BU(k) + W(k) \\ Z(k) = HX(k) + V(k) \end{cases} \quad (1)$$

Where A is the one-step transfer matrix from time k-1 to time k, $W(k)$ is the system noise, H is the measurement matrix, and $V(k)$ is the measurement noise. In step (2), the predicted center point coordinates are the predicted values of Kalman filter model and the center coordinates of the light bar in the normal direction of the predicted point calculated in step (3) are the observed values of the Kalman filter model. In addition, it is assumed that $W(k)$ and $V(k)$ are uncorrelated and both are Gaussian white noise.

In the process of predicting the center of the light bar, because the prediction step is very small, it can be assumed that the center of the light bar is in the direction of the ridge. According to the prediction point described in step (2), the state one-step prediction is described as follows:

$$P(k) = S(k-1) + BU(k) \quad (2)$$

$S(k-1)$ is the coordinates of the center point of the light bar at k-1 step, $P(k)$ is the center point of the predicted light bar of the k step, $U(k)$ is the ridge direction, and B is the ridge trace step size matrix. If the step is 1, B is a two-dimensional unit matrix.

Predictive mean square error and filter gain expression as shown in equations (3) and (4). Q and R are the self-covariance matrices of Gaussian white noise $W(k)$ and $V(k)$ respectively, and the initial value of the mean square error matrix is set to $[1,1]^{T}$.

$$C(k \mid k-1) = C(k \mid k-1) + Q \quad (3)$$

$$kg(k) = C(k \mid k-1) / (C(k \mid k-1) + R) \quad (4)$$

The center point of the light bar is estimated as shown in equation (5), where $S(k)$ is the center point of the k step, and the center point estimate S_k is the true value of the center of the light bar.

$$S(k) = P(k) + kg(k)[Z(k) - P(k)] \quad (5)$$

The mean square error estimate is updated as shown in equation (6).

$$C(k \mid k) = (1 - kg(k))C(k \mid k-1) \quad (6)$$

Step 5: Ridge line forecast direction update

As the step size is very small, and the direction of the track bar does not sudden change, then the current light bar center point vector is used to the next step of the ridge line prediction direction.

Repeat steps 1 to 5 above until the termination condition is met. It means the forecast point reaches the light bar boundary. The partial curve of the estimated value S_k of the light bar center extracted by the method described in this paper is compared with the partial curve of the observed value Z_k as shown in Fig. 9. The red curve is the observed value Z_k and the blue curve is the estimated value S_k. From the comparison results can be seen, Kalman filter can effectively filter out part of the noise, making the extracted light bar centerline closer to the true value.

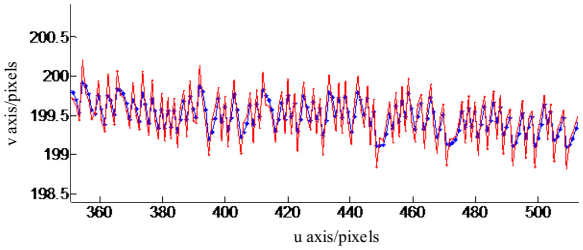

Fig. 9. Comparison of estimated and observed values.

The center of the light bar extracted by the method described in this paper is compared with the center of the light bar extracted by the grayscale method of the column direction, as shown in Fig. 10. A straight line fitted with the light bar center as a baseline. The mean and mean square errors of the center point respectively extracted by the two methods are calculated as shown in Table 1. According to the statistical results shown in Table 1 can be seen, the method described in this paper is more accurate for extracting the light bar center.

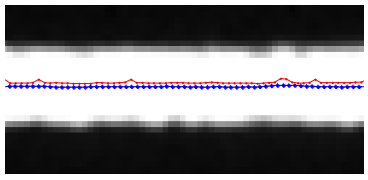

(a) Light bar center extraction by different methods

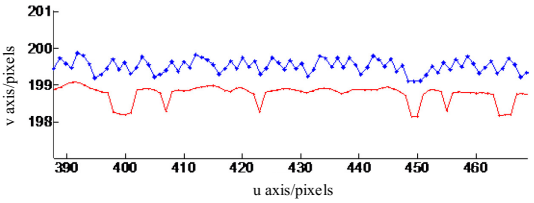

(b) Local enlargement of light bar center comparison

Fig. 10. Light bar center extraction comparison.

TABLE I
LIGHT BAR CENTER EXTRACTION ERROR STATISTICS TABLE

The method of this paper		Column direction gray center of gravity	
error mean	mean square error	error mean	mean square error
0.205	$1.692*10^{-5}$	3.264	0.021

V. F-TRACK SEAM FEATURE EXTRACTION

A. F-track image feature analysis

Medium-low speed maglev F-track detection is divided into vertical F-track seam detection, end F-track seam detection and horizontal F-track seam detection. The light plane projection of the laser camera sensor for vertical F-track seam detection and end F-track seam detection is shown in Fig. 11 (a). The structure of the light plane perpendicular to the F-track suspension clearance detection surface, forming a structure

along the rail line light bar. The camera collect the light bar image shown in Fig. 12. The structure of the light plane is projected horizontally on the side of the external magnetic pole and The F-type track on both parts of the track slits have a chamfering structure, as shown in Fig. 11 (b). The light bar image acquired by the camera is shown in Fig. 13.

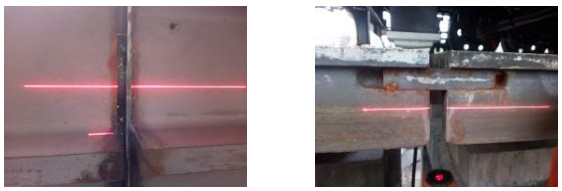

(a) Vertical/end track seam light bar (b) Horizontal track Light bar

Fig. 11. Light bar physical map.

Fig. 12. Vertical / End Track seam light bar Image.

Fig. 13. Horizontal track light bar image.

According to the geometric characteristics of the F-track seam and the characteristics of the track light bar images collected by the cameras, the F-track seams can be abstracted into four cases. As shown in Fig. 14, the red dots are the track seam feature points.

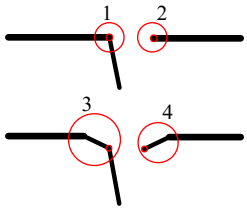

Fig. 14. Schematic diagram of the F-track seam.

According to the curve of the light bar image was linearly distributed, the method of extracting the light bar center proposed in this paper can be simplified, that is, the direction of the initial ridge line is given horizontal direction, and the direction of the ridge line prediction is discretized. The discretized predicted ridge direction θ_k satisfies the segmentation function shown in equation (7). The remaining steps remain unchanged.

$$\theta_k = \begin{cases} \theta_{l_0} & T_1 \le \theta_k < T_2 \\ \theta_{l_1} & T_2 \le \theta_k < T_3 \\ \theta_{l_2} & T_3 \le \theta_k < T_4 \end{cases} \tag{7}$$

θ_{l_i} $(i = 0,1,2)$ represents the direction of the ridge line according to the prior knowledge, and T_i $(i = 0,...4)$ represents the threshold of discretization.

B. Light bar center line fitting

The method used to fit the straight line is the least squares method. The hypothesis function $f(u) = ku + b$ (k and b are parameters) and the sample is the center of the light bar (u_i, v_i) $(i = 1,2,\cdots n)$, so the objective function is

$$s = \sum_{i=1}^{n} [v_i - f(u)]^2 \tag{8}$$

When the objective function takes the minimum value, the resulting straight line equation is the best empirical formula. There are linear equations for the parameters k and b.

$$\begin{cases} \dfrac{\partial s}{\partial k} = -2\sum_{i=1}^{n}(v_i - b - ku_i)u_i = 0 \\ \dfrac{\partial s}{\partial b} = -2\sum_{i=1}^{n}(v_i - b - ku_i) = 0 \end{cases} \tag{9}$$

Equation (9) is expressed in matrix form

$$\begin{bmatrix} \sum_{i=1}^{n} u_i^2 & \sum_{i=1}^{n} u_i \\ \sum_{i=1}^{n} u_i & n \end{bmatrix} \begin{bmatrix} k \\ b \end{bmatrix} = \begin{bmatrix} \sum_{i=1}^{n} u_i v_i \\ \sum_{i=1}^{n} v_i \end{bmatrix} \tag{10}$$

Solution is

$$\begin{bmatrix} k \\ b \end{bmatrix} = \begin{bmatrix} \sum_{i=1}^{n} u_i^2 & \sum_{i=1}^{n} u_i \\ \sum_{i=1}^{n} u_i & n \end{bmatrix}^{-1} \begin{bmatrix} \sum_{i=1}^{n} u_i v_i \\ \sum_{i=1}^{n} v_i \end{bmatrix} \tag{11}$$

So that

$$\begin{cases} k = \dfrac{\sum_{i=1}^{n} u_i \sum_{i=1}^{n} v_i - n\sum_{i=1}^{n} u_i v_i}{(\sum_{i=1}^{n} u_i)^2 - n\sum_{i=1}^{n} u_i^2} \\ b = \dfrac{\sum_{i=1}^{n} u_i v_i \sum_{i=1}^{n} u_i - \sum_{i=1}^{n} v_i \sum_{i=1}^{n} u_i^2}{(\sum_{i=1}^{n} u_i)^2 - n\sum_{i=1}^{n} u_i^2} \end{cases} \tag{12}$$

In order to reduce the interference of the noise to the center of the light bar, the sample points can be subjected to multiple least squares fitting. Each time the straight line equation is obtained, the sample point is filtered. If the distance from the center point of the light bar to the straight line is larger than the preset threshold, the point is considered as noise, and the point is excluded when fitting straight line next time. Usually twice least squares straight line fitting can meet the requirements.

C. Feature points extraction of F-track seam image

In this paper, a feature point extraction method is proposed according to the four kinds of F-track seam feature points shown in Fig 14. The feature points shown in cases 1 and 3 are extracted using the threshold segmentation line fitting method (abbreviation is TSFM), and the feature points are shown in cases 2 and 4 using the deviation threshold method (abbreviation is DTM) to extract.

(1) Threshold segmentation line fitting method (TSFM)

TSFM of F-track seam feature point extraction steps are as follows:

Step 1: Two horizontal stripes are selected according to the position of the light bar at the end of F-track seam. The line of the selected light bar center line is fitted by TSFM to obtain a fitting straight line $y_1(x)=k_1x+b_1$.

Step 2: The center line of the light bar is searched from the end point of F-track seam. And the vertical distance h of the center points of the light bar to the reference line (ie, the straight line $y_1(x)=k_1x+b_1$) are calculated. Then the center point of the light bar which satisfied the condition $Min_{Th}<h<Max_{Th}$ are selected to form a new column P_1, where Min_{Th} and Max_{Th} are the selected upper and lower thresholds. When the number of coordinate points in the column P_1 contains more than M, the line P_1 is fitted in a straight line to obtain a fitting straight line $y_2(x)=k_2x+b_2$.

Step 3: If the column P_1 in step 2 does not meet the requirement, it is considered to be the form of the F-track seam feature point shown in case 2. If the column P_1 in step 2 satisfies the condition, then repeating step 2 to get the point column P_2 with straight line $y_2(x)=k_2x+b_2$ as the reference line. If the column P_2 satisfies the requirement, it is considered to be the case 3. And the straight line is fitted with the column P_2 to obtain the straight line equation $y_3(x)=k_3x+b_3$. Find the intersection of lines $y_2(x)=k_2x+b_2$ and $y_3(x)=k_3x+b_3$ as the feature points. If the point P_2 does not satisfy the requirement and the slope k_2 of the straight line $y_2(x)=k_2x+b_2$ is greater than a fixed threshold T_k, it is considered to be the form of the F-track seam feature point shown in the case 1, then find the intersection of straight lines $y_1(x)=k_1x+b_1$ and $y_2(x)=k_2x+b_2$ as the feature points. Otherwise it is considered to be the form of the F-track seam feature point shown in the case 4.

(2) deviation threshold method(DTM)

The TSFM process separates the feature points of case 2 and case 4, then using different thresholds to extract the feature points. The extraction method is as follows:

For the case 2, the line $y_1(x)=k_1x+b_1$ is the reference line, traversing from the end of the track to the center of the bar, and calculating the vertical distance of the traversing point to the reference line, then selecting the feature point through the appropriate threshold T_h.

For the case 4, the straight line $y_1(x)=k_1x+b_1$ obtained in step 1 of TSFM is used as the reference line to calculate the distance from the point on the straight line $y_3(x)=k_3x+b_3$ to the reference line, and the appropriate threshold value T_h is selected to obtain the F-track seam feature point.

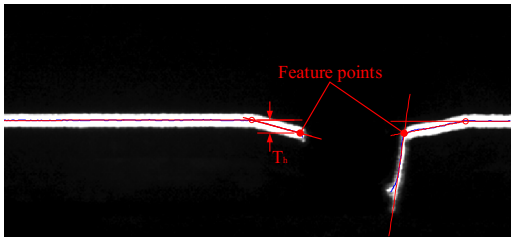

(a) Case 3 and 4 seam feature point extraction

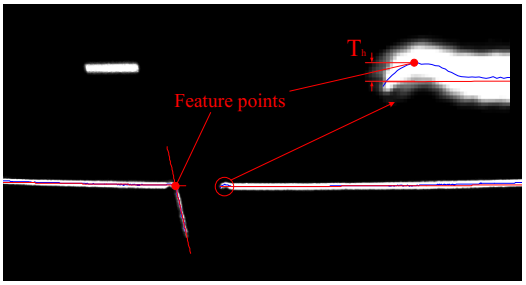

(b) Case 1 and 2 seam feature point extraction

Fig. 15. Seam feature extraction.

D. Calculation of F-track seam

According to the camera calibration in Section 2.2 and the feature points of Section 4.3, we can get the coordinates of the feature points in the corresponding world coordinate system, and the corresponding geometrical parameters can be calculated accordingly.

The world coordinate system $O_{W1}X_{W1}Y_{W1}$ corresponding to the laser camera type sensor for horizontal F-track seam detection is shown in Fig. 16. The coordinates of image point C and D of the F-track points extracted from section 4.3 are taken into the camera calibration model to obtain the coordinates of $C(x_{C-W},y_{C-W})$ and $D(x_{D-W},y_{D-W})$ in the world coordinate system. Then the horizontal F-track seam can be calculated as shown in equation (13), where l is the horizontal seam deviation.

$$l=\left|x_{C-W}-x_{D-W}\right| \tag{13}$$

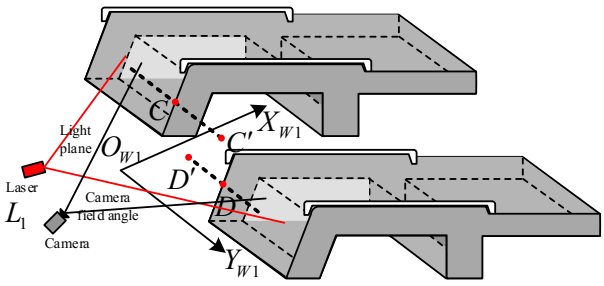

Fig. 16. Schematic diagram of the horizontal seam detection coordinate system

The world coordinate system $O_{W1}X_{W1}Y_{W1}$ corresponding to the laser camera type sensor for vertical F-track seam and end of F-track seam detection is shown in Fig. 17. The coordinates of image point A and B of the F-track seam points extracted from section 4.3 are taken into the camera calibration model to obtain the coordinates of $A(x_{A-W},y_{A-W})$ and $B(x_{B\text{-}W},y_{B\text{-}W})$ in the world coordinate system. The vertical F-track seam and the end of F-track seam are calculated as shown in Eq. (14) and (15), where h is the vertical F-track seam deviation and s is the end of F-track seam deviation.

$$h=\left|x_{A-W}-x_{B-W}\right| \tag{14}$$

$$s=\left|y_{A-W}-y_{B-W}\right| \tag{15}$$

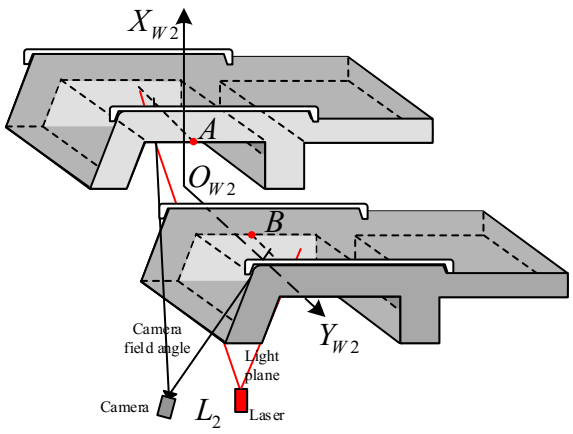

Fig. 17. Schematic diagram of the coordinate system for the vertical and end F-track seam.

VI. TEST

A. Light Bar Center Extraction Comparison Test

Detection vehicle slowly through the F-track seam which randomly selected in the line, and the sensor acquires the F-track image under different viewing angles with acquiring rate of 200f/s, finally obtains 30 available F-track seam images. For the same track under different angles images, the Kalman filter algorithm based on the ridge prediction and the gray center of gravity algorithm are used to extract the center of the light bar. Then the end of F-track seam is calculated by the method described in Section 4. Finally the end of F-track seam measurement results by different algorithm curve are obtained, the results shown in Fig. 18. The means of results of the two algorithms are 23.72mm and 23.53mm respectively, and the manual measurement result of the end of F-track seam is 23.86mm. From the comparison between the comparison curve, the measured mean value and the manual measurement value, it can be seen that the method of extracting the light bar in this paper has better stability and higher accuracy for the same end of F-track seam in different angles.

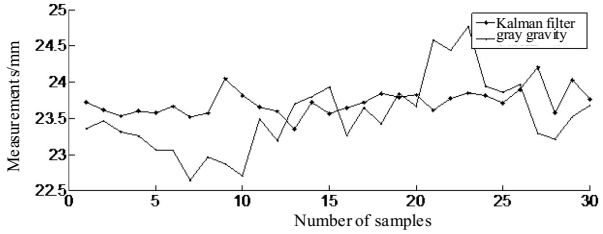

Fig. 18. Contrast curve of end F-track seam.

B. Test Stability Verification Experiment

The stability of the F-track seam detection system is verified under laboratory conditions. The simulation F-track seam is measured with a simple test platform, as shown in Fig. 19. The experiment was carried out under laboratory conditions using the detection system to simulate the F-track seam. The experimental procedure was as follows: the seam was kept constant, measured once every minute, and the end, horizontal nd vertical F-track seams were measured 15 times.

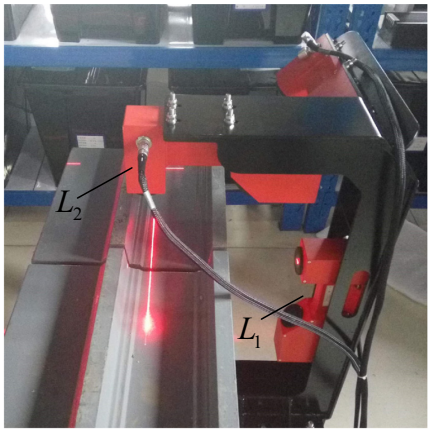

Fig. 19. F-track seam test platform.

The results of the end F-track seam test are shown in Fig. 20. The mean value of the sample data is 19.34mm, the standard deviation is 0.032mm, and the maximum deviation between the sample data and the sample mean is 0.072mm.

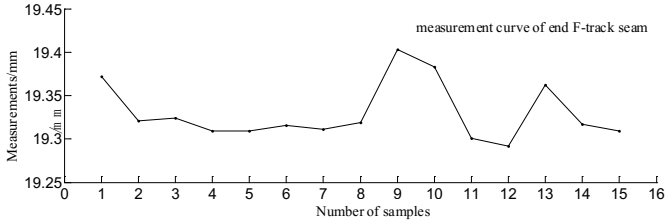

Fig. 20. Measurement curve of end F-track seam.

The results of horizontal F-track seam test are shown in Fig. 21. The mean value of the sample data is 0.76mm, the standard deviation is 0.016mm, and the maximum deviation between the sample data and the sample mean is 0.044mm.

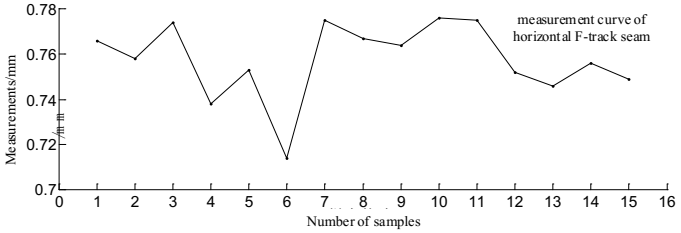

Fig. 21. Measurement curve of horizontal F-track seam.

The results of vertical F-track seam test are shown in Fig. 22. The mean value of the sample data is 1.24mm, the standard deviation is 0.045mm, and the maximum deviation between the sample data and the sample mean is 0.083mm.

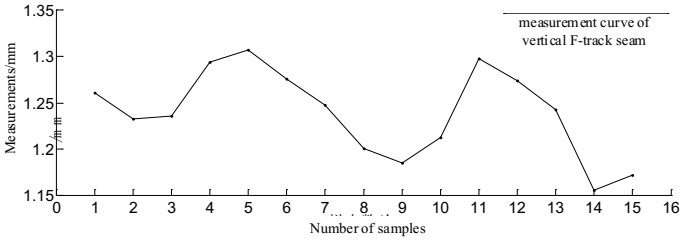

Fig. 22. Measurement curve of Vertical F-track seam.

C. Detection accuracy verification experiment

The verification accuracy test is divided into static detection accuracy verification and dynamic detection accuracy

verification. Detection system is installed in the medium-low speed magnetic comprehensive detection vehicle. Verification experiment is completed in the medium-low speed maglev test line which is in the vehicle Zhu Zhou Electric Locomotive Co. Ltd. , as shown in Fig. 23.

Fig. 23. Medium-low speed maglev comprehensive detection vehicle.

Static accuracy verification test process is to select five F-track seam in the medium-low speed maglev line randomly, then the detection vehicle in turn stopped at the top of the selected seams for measuring the parameters of the end, the horizontal and the vertical F-track seam under the static condition of the detection vehicle. Finally the measured result of the system compared with the manual measurement to verify the accuracy of the detection system.

The results of the static test accuracy of the F-track seam are shown in Table II, Table III and Table IV. The manual measurement of the end F-track seam is measured by a caliper with the precision of 0.02 mm, as shown in Fig. 24. Horizontal and vertical F-track seam are measured by a steel ruler and filler gauge, as shown in Fig. 25.

Fig. 24. Measurement of end F-track seam.

（a）Measurement of Horizontal F-track seam（b）Measurement of Vertical F-track seam

Fig. 25. Horizontal and vertical F-track seam measurement.

TABLE II
STATIC ACCURACY VERIFICATION OF END RAIL JOINTS

num	item	Measure-ments（mm）	standard (mm)	error (mm)	error mean (mm)
1	end seam	18.396	18.20	0.196	0.137
2		21.208	21.38	0.172	
3		17.863	18.02	0.157	
4		18.771	18.80	0.029	
5		29.369	29.50	0.131	

TABLE III
HORIZONTAL F-TRACK SEAM STATIC ACCURACY VERIFICATION

num	item	Measure-ments（mm）	standard (mm)	error (mm)	error mean (mm)
1	Horiz-ontal seam	0.310	0.18~0.20	0.120	0.088
2		1.127	0.90~1.00	0.177	
3		0.017	0.02~0.03	0.008	
4		0.517	0.45~0.50	0.042	
5		2.043	1.90~2.00	0.093	

TABLE IV
VERTICAL F-TRACK SEAM STATIC ACCURACY VERIFICATION

num	item	Measure-ments （mm）	standard (mm)	error (mm)	error mean (mm)
1	Verti-cal seam	0.197	0.18~0.20	0.007	0.040
2		0.648	0.65~0.68	0.017	
3		0.386	0.45~0.50	0.089	
4		0.403	0.40~0.45	0.072	
5		0.811	0.80~0.85	0.014	

Table III, IV horizontal and vertical F-track seam standard value using the feeler measurement, such as the standard value of 0.18 ~ 0.20 said 0.18mm feeler can be inserted into the gap, 0.20mm feeler can not be inserted into the gap, and then take their average value for the standard value. The error is the difference between the measured value and the standard value.

The accuracy of the dynamic detection test is intended to verify the repeatability of the detection system. The repeatability accuracy means that the error value between the two measuring points of the same section is measured at same speed, same direction and same operating environment. Due to the constraints of the experimental line conditions, this paper discusses the dynamic accuracy of the experimental speed of 10km / h. The results of the two dynamic measurements of the left F-track seam of the running direction were selected for statistical analysis of repeatability accuracy.

The results of the two dynamic test results are shown in Fig. 26. The repeatability curve is shown in Fig. 27. The maximum value of the error is 0.581mm, the repeatability precision is -0.034mm, and the standard deviation is 0.273mm.

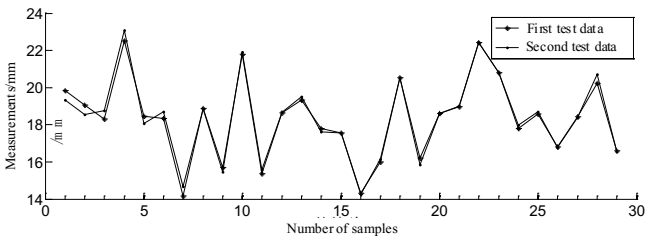

Fig. 26. Measurement curve of end F-track seam.

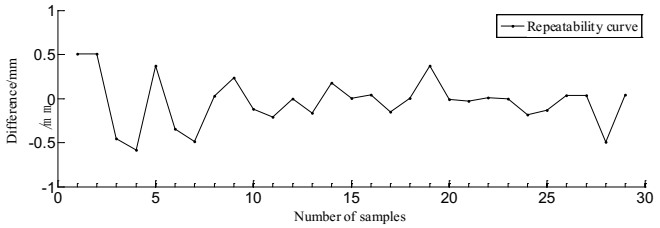

Fig. 27. The repeatability precision curve of the end F-track seam.

The horizontal seam of the two dynamic test results are shown in Fig. 28. The repeatability curve is shown in Fig. 29. The maximum value of the error is -0.170mm, the repeatability precision is -0.001mm, and the standard deviation is 0.076mm.

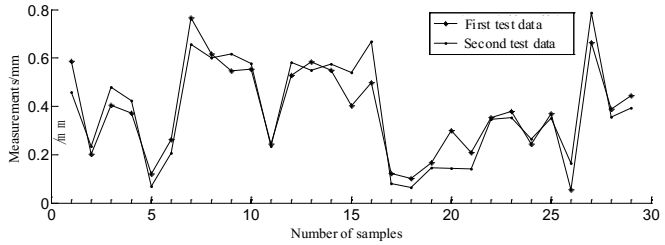

Fig. 28. Measurement curve of horizontal F-track seam.

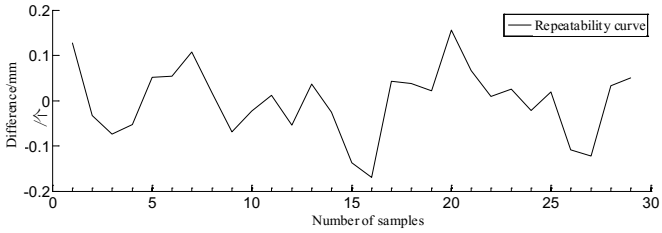

Fig. 29. The repeatability precision curve of horizontal F-track seam.

The vertical seam of the two dynamic test results are shown in Fig. 30. The repeatability curve is shown in Fig. 31. The maximum value of the error is -0.391mm, the repeatability precision is -0.021mm, and the standard deviation is 0.123mm.

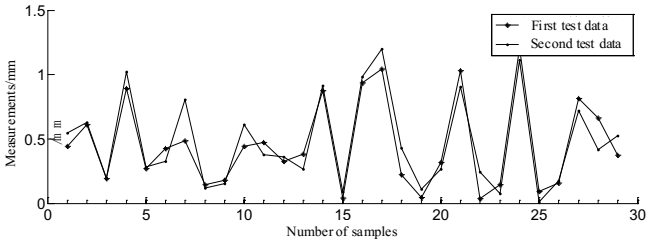

Fig. 30. Measurement curve of Vertical F-track seam.

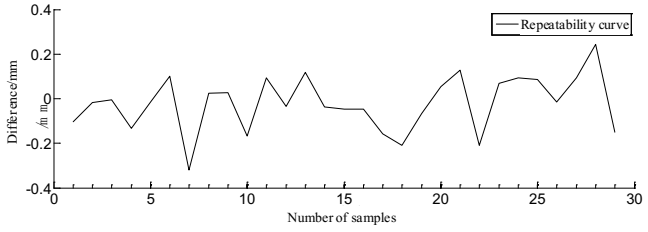

Fig. 31. The repeatability precision curve of Vertical F-track seam.

D. Accuracy verification experiment with different speed

Detected the same line twice at different speeds (10km/h and 20km/h) and compared the results to verify the accuracy of detection.

The results of the two dynamic test results with different speed are shown in Fig. 32. The difference is shown in Fig. 33. The maximum value of the difference is 1.452mm and the mean of absolute value of difference is 0.773mm.

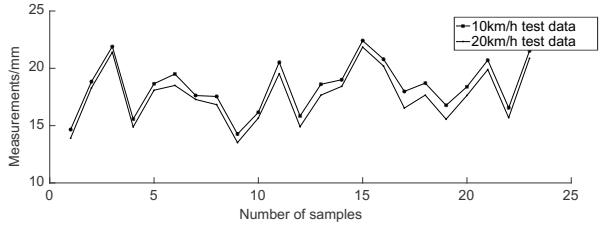

Fig. 32. Measurement curve of end F-track seam in different speed.

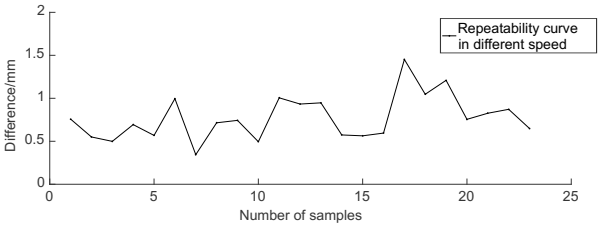

Fig. 33. The difference between the two measurements of end F-track seam in different speed.

The horizontal seam of the two dynamic test results with different speed are shown in Fig. 34. The difference is shown in Fig. 35. The maximum value of the difference is 0.206mm and the mean of absolute value of difference is 0.084mm.

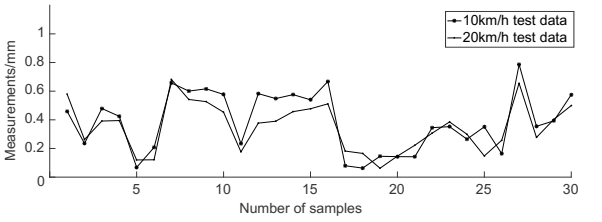

Fig. 34. Measurement curve of horizontal F-track seam in different speed.

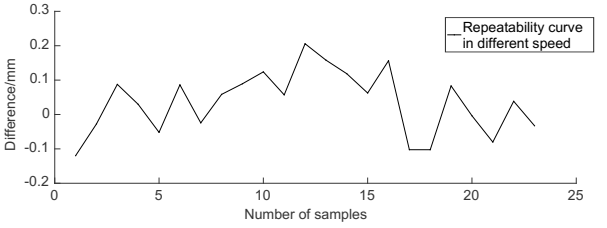

Fig. 35. The difference between the two measurements of horizontal F-track seam in different speed.

The vertical seam of the two dynamic test results with different speed are shown in Fig. 36 The difference is shown in Fig. 37. The maximum value of the difference is 0.289mm and the mean of absolute value of difference is 0.106mm.

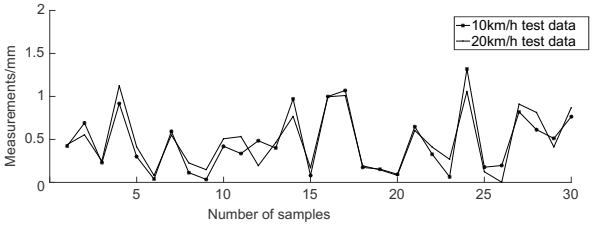

Fig. 36. Measurement curve of vertical F-track seam in different speed.

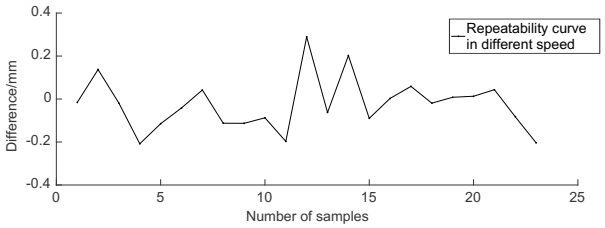

Fig. 37. The difference between the two measurements of vertical F-track seam in different speed.

VII. Conclusion

(1) The influence of the medium-low speed maglev F-track structure, the geometrical parameters of the F-track and the abnormal of F-track seam on the operation of the maglev train are discussed.

(2) This paper presents a structure of medium-low speed maglev F-track seam detection system based on machine vision detection technology.

(3) The method of image processing is studied, and a Kalman filter light bar center extraction method based on ridge line prediction and F-track seam feature point extraction method are proposed to realize the dynamic detection of F-track seams.

(4) The feasibility of the method is proved by the relevant experiments. The static accuracy of the end F-track seam is less than 0.5mm, and the dynamic accuracy is less than 0.8mm. Then the static accuracy of the horizontal F-track seams is less than 0.2mm, the dynamic precision is less than 0.5mm. And the static accuracy of the vertical F-track seams is less than 0.2mm, the dynamic accuracy is less than 0.5mm. The test results show that the detection accuracy meets the design requirements.

(5) Detection speed has no effect on horizontal and vertical F-track seam measurement, however it will have some impact on the detection of end F-track seam. The detection results of end F-track seam in 20km/h are lower than the results in 10km/h. It is because image smear cause the end F-track seam to be narrower in the light bar image. But this effect is not serious.

References

[1] Cai Wen feng, Yan Hua, Yang Ping. “Analysis of the Characteristics and Engineering Adaptability of Track System for Medium and Low Speed Maglev Transit”. *Journal of railway engineering society*, vo. 32, no. 2, pp. 54-59, 2015.

[2] Hu Li feng. “Development of Static Geometric Parameter Detector for Low Speed Maglev F-type track”, Central South University, 2011.

[3] Zheng Shu bin, Lin Jian hui, Lin Guo bin. “Implementa -tion of Detecting Maglev Track Long Wave Irregularity Based on Inertial Measurement Principle”. *Journal of Electronic Measurement and Instrument*, vo. 21, no. 1, pp. 61-65, 2007.

[4] Wang Yue ting. “Guide-way Monitor System of Shanghai Maglev Track Linear”. *Urban Mass Transit*, vo. 18, no. 6, pp. 123-125, 2015.

[5] Zhou Wen wu, Wu Jun, Li Zhong xiu et al. “A Track Geometry Measurement System for Low Speed Maglev”. *Journal of National University of Defense Technology*, vo. 18, no. 6, pp. 123-125, 2015..

[6] Wei Shi bin, Liu Ling ping, Zhao Yan feng, et al. “Track Inspection System of Type GJ-4”. *Railway Engineering*, vo.11, pp. 98~101, 2011.

[7] Zhan Dong, Yu Long, Xiao Jian. “The Calibration Approach Study on the Multiple Vision Sensors for Railway Tunnel Clearance Full Cross-section Inspection”. *Journal of The China Railway Society*, vo. 37, no. 7, pp. 98-106, 2015.

[8] Zhan Dong, Yu Long, Xiao Jian, et al. “High-Speed and Dynamic Vision Measurement Approach Study for Overhead Catenary System Geometric Parameters Inspection”. *Chinese Journal of Scientific Instrument*, vo. 35, no. 8, pp. 1852-1859, 2014.

[9] Zhan Dong, Yu Long, Xiao Jian, et al. “A High-accuracy Vision Measurement Approach Study for Rail Full Cross-sectional Profile Dynamic Inspection”. *Journal of The China Railway Society*, vo. 37, no. 9, pp. 96-106, 2015.

[10] Sun Jun hua, Wang Heng, Liu Zhen, et al. “Rapid extraction algorithm of laser stripe center in rail wear dynamic measurement”. *Optics and Precision Engineering*, vo. 19, no. 3, pp. 690, 2011.

[11] Wang Jin qiao, Duan Fa jie, Feng Fan, et al. “Extraction Method of Structured Light Stripe Center Based on AACMM Laser Scanning System”. *Opto-Electronic Engineering*, co. 42, no. 1, pp. 13-19, 2015.

[12] Hu Li feng, Ying Li jun, Wu Zhi xiang. “Overview of track geometry of medium low speed maglev train”. *Entrepreneur World*, no.1, pp. 67-68, 2011.

[13] Zhan Dong, Yu Long, Xiao Jian, et al. “Study on vehicle vibration compensation in railway track profile inspection”. *Chinese Journal of Scientific Instrument*, vo. 34, no. 7, pp. 1625-1633, 2013.

[14] Weng Ju yang, P. Cohen, M. Herniou. “Camera calibration with distortion models and accuracy evaluation”. *IEEE Trans. on Pattern Analysis and Machine Intelligence*, vo. 14, no. 10. Pp. 965-980, 1992.

[15] Li Guo xin, Wang Chong lin, Liu Jian hua, et al. “Dynamic rail-wear inspecting system based on machine vision”. In *2007 Second IEEE Conference on Industrial Electronics and Applications*, pp. 1-4, 2007.

[16] Zhang Guang jun. *Vision measurement*. Beijing: Science Press, 2008.

Dongkai Zhang received the B.S. degree in electrical engineering from Henan University of Science and Technology, LuoYang, China, in 2010, and the M.S. degree in Electrical Engineering from Southwest Jiaotong University, Chengdu, China, where he is currently working toward Ph.D. degree in Electrical Engineering.

His research interest includes machine vision inspection technology and fault diagnosis and fault prediction of image processing based on statistical learning and depth learning.

Shibin Gao received the B.S., M.S. and Ph.D. degrees in Electrical Engineering from Southwest Jiaotong University, Chengdu, China, in 1985, 1988 and 2004, respectively.

Form 1993 to 1998, he was an Assistant Professor with the Electrical Engineering Department, Southwest Jiaotong University. Since 1998, he has been a Professor with the Electrical Engineering Department, Southwest Jiaotong University. He twice won the national scientific and technological progress second prize in 2012 and 2013. He is the author of seven books and more than 100 articles. His research interests include railway transportation traction power supply system automation, safety of traction power supply system for rail transit, power system relay protection and substation

integrated automation and on-line monitoring of electrical equipment.

Long Yu received the B.S., M.S. and Ph.D. degrees in Electrical Engineering from Southwest Jiaotong University, Chengdu, China, in 2003, 2006 and 2008, respectively.

Form 2009 to 2012, he was a lectorate with the Electrical Engineering Department, Southwest Jiaotong University. Since 2012, he has been an Assistant Professor with the Electrical Engineering Department, Southwest Jiaotong University. He is the author of 47 articles. His reasearch interests include fault diagnosis and fault prediction of image processing based on statistical learning and depth learning, mechanical and electrical signal detection and processing, intelligent measurement and control technology and simulation of catenary modeling.

Dong Zhan received the B.S. degree in electrical engineering from Jiangxi University of Science and Technology, Nan Chang, China, in 2009, and the M.S. and Ph.D degrees in electrical engineering from Southwest Jiaotong University, Chengdu, China, in 2012 and 2016, respectively.

His research interest includes machine vision inspection technology and fault diagnosis.